Implementation of Fault Ride-Through Techniques of Grid-Connected Inverter for Distributed Energy Resources With Adaptive Low-Pass Notch PLL

Dongsul Shin, *Student Member, IEEE*, Kyoung-Jun Lee, *Student Member, IEEE*, Jong-Pil Lee, *Member, IEEE*, Dong-Wook Yoo, *Member, IEEE*, and Hee-Je Kim

***Abstract*—The amount of distributed energy resources (DERs) has constantly increased worldwide. As the power ratings of DERs have become considerably high, the grid code requirements are necessary to secure reliable power generation and transmission for the public electric network. In order to follow grid codes of the various countries and optimize the function of grid-connected inverters for DERs, a robust phase-locked loop (PLL) is essential for extracting the grid phase information accurately, when the grid voltage is polluted by harmonics and unbalanced. This paper proposes fault ride-through techniques based on a low-pass notch (LPN)-PLL. The LPN-PLL has not only fast and smooth transient responses to a sudden transition of the grid voltage but also has robustness to the distorted and unbalanced grid conditions. Therefore, the stable performance in the grid fault conditions is expected without the system trip. Furthermore, a universal voltage sag generator for the various grid codes with six parameters is proposed for the verification of low voltage ride-through (LVRT) performance. Experimental verifications are presented to show the LVRT performance based on the LPN-PLL with a three-phase grid-connected inverter (10 kV·A) and a prototype of the voltage sag generator (10 kV·A).**

***Index Terms*—Distributed energy resources (DER), fault ride-through (FRT), grid codes, low-pass notch (LPN) filter, low voltage ride-through (LVRT), phase-locked loop (PLL).**

I. INTRODUCTION

DISTRIBUTED generations based on renewable green energies are expected to increase at a surprising rate, and simultaneously change the electric power generation paradigm [1], [2]. Consequently, the increasing penetration of distributed generations (DGs) to the power grid has introduced stability problems [3] and reinforced existing concerns regarding their influences on the grid stability among transmission system operators (TSOs) [4]. Before 2003, there were no requirements from utility grids for LVRT or fault ride-through (FRT) performance of wind turbine generator systems (WTGSs), however, in that year, E.ON-Netz of Germany was the first to implement those needs into their grid code [5]–[7]. According to the guideline of the grid code, WTGS needs to be on-grid and provide reactive power into the grid. Only when the grid voltage drops below the guideline of the grid code, WTGS is disconnected from the grid [8], [9]. Also, FRT for photovoltaic (PV) plants was mentioned in the German grid code from January 1st 2011; PV plants have to be capable to participate in full dynamic network support during grid faults: To stay connected to the network and provide voltage support by injecting a reactive current into the grid. Therefore, in order to fulfill these requirements for the grid stability, the performance of DG systems must be improved to meet the grid codes in each country.

To provide uninterrupted service in the face of grid disturbances, advanced methods for fast and accurate synchronization of the grid voltage are required. In grid-connected applications, the PLL is the first step to the any controller. Especially, in the FRT condition, a robust PLL method is required to guarantee the performance of controllers for the grid-connected inverters. The synchronous reference frame (SRF)-PLL method has been used most widely for the grid synchronization [10], [11]. Under the ideal grid condition, the SRF-PLL with the high bandwidth feedback loop shows the fast and accurate PLL performance [12]. However, the SRF-PLL method is quite sensitive to the distorted and unbalanced conditions [13]–[15]. Many researchers have examined the ways of improving the conventional SRF-PLL including double synchronous reference frame-PLL [16], [17], SRF-PLL with a sinusoidal signal integrator-PLL [18], double second-order generalized integrator (DSOGI)-PLL [19], and decoupled double synchronous reference (DDSRF)-PLL [20]. decoupled double synchronous reference frame (DDSRF)-PLL exploits two SRFs rotating at the fundamental grid frequency to detect the positive- and negative-sequence components of the grid voltage under the unbalanced grid faults. Similarly, double second order generalized integrator (DSOGI)-PLL adopts the instantaneous symmetrical component method on the $\alpha\beta$-axis stationary reference frame. Although the aforementioned PLL methods show the good performances, the implementation of these algorithms is quite complicated and the dynamic response is not fast due to the proportional-integral (PI)-based controller. Besides, the PLL methods based on the principle of delayed signal cancelation[21]–[23] have been proposed to detect and eliminate any specified harmonic components. However, these methods require multiple digital signal processors (DSPs) to reduce the execution time of the algorithms.

Manuscript received December 16, 2013; revised October 1, 2014; accepted November 10, 2014. Date of publication December 10, 2014; date of current version December 23, 2014. Recommended for publication by Associate Editor F. W. Fuchs.

D. Shin is with the Department of Electrical Engineering, Pusan National University, Busan 609-735, Korea (e-mail: jirubak762@keri.re.kr).

K.-J. Lee is with the High-Power Testing Department, Korea Electro technology Research Institute, Changwon 641-120, Korea (e-mail: kyoungjun@keri.re.kr).

J.-P. Lee and D.-W. Yoo are with the Power Conversion Center, Korea Electro technology Research Institute, Changwon 641-120, Korea (e-mail: jplee@keri.re.kr; dwyoo@keri.re.kr).

H.-J. Kim is with the Department of Electrical Engineering, Pusan National University, Busan 609-735, Korea (e-mail: heeje@pusan.ac.kr).

Digital Object Identifier 10.1109/TPEL.2014.2378792

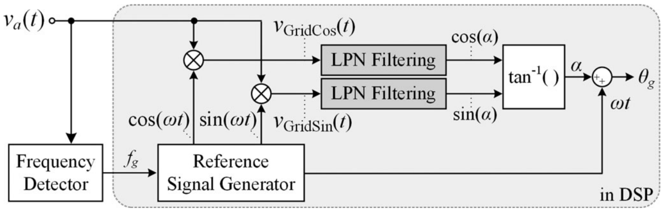

Fig. 1. Block diagram of the proposed PLL method. $v_a(t)$ is the phase A voltage of the three-phase grid voltage.

Unlike the SRF-based PLL algorithms, the PLL method using the fast Fourier transform (FFT) concept (designated FFT-PLL) does not require a PI controller [13], [15]. The FFT-PLL shows the good PLL performance under harmonic-distorted conditions. In addition, the gain tuning of PI controller is not required to adjust the dynamic performance. However, when the phase jump of the grid voltage happens, it takes one period to be locked completely to the new phase angle of the grid voltage. During this transient time, faulty information on the phase angle of the grid voltage deteriorates the quality of the power injected into the grid at the point of common coupling (PCC), resulting in unacceptable current distortion [24]. Therefore, research on how to improve the performance of the PLLs for the polluted and suddenly changing grid is a very important issue.

On the other hands, many studies have examined advanced control schemes regarding the operation of the grid-connected inverters under balanced or unbalanced grid fault conditions [5], [25]–[28]. Most voltage sags caused by utility faults include positive-, negative-, and zero-sequence components [6]. For this reason, in order to support the grid voltage restoration properly, the positive- and negative-sequence currents should be considered in current control loops. In SRF, a vector current controller with feedforward of negative-sequence grid voltage (VCCF) was implemented in the positive-sequence reference frame [29], [30]. With feedforward of negative-sequence voltage, only positive-sequence dq-axis currents flow into the grid (i.e., negative-sequence currents cannot be controlled). Therefore, in order to control the negative-sequence currents, a dual vector current control (DVCC) algorithm was proposed [29], [31]–[33]. The positive- and negative-sequence dq-axis currents are controlled in individual SRFs. On the other hands, in stationary reference frame, the $\alpha\beta$-axis currents are controlled by the current references with reflection of the positive- and negative-sequence components [4]. While the control strategies for the LVRT performance have been examined in many studies [4], [6], [34], the LVRT strategy to increase the reliability for keeping the connection to the faulty grid with consideration for the PLL method has not been presented. Especially, in the SRF, the phase angle from the PLL is used to transform the reference frames. When the unbalanced voltage sags that lead to the phase jump happen, the PLL generates a sudden change in the phase angle. This makes an adverse effect on the current controllers. For this reason, the PLL method should be considered for the LVRT strategy. Also, at the final stage of development of the grid-connected inverters, the voltage sag generator to evaluate the LVRT performance is required.

In this paper, an adaptive LPN-PLL is adopted for the FRT operation of the grid-connected inverter. The LPN-PLL has not only fast and smooth transient responses to a sudden transition of the grid voltage but also has robustness to the distorted and unbalanced conditions. With this characteristic of LPN-PLL, the stable performance in the grid fault conditions is guaranteed without the system trip. For the proper response of the unbalanced FRT conditions and the improvement of the reliability, the current controllers with the DVCC for the injection of positive- and negative-sequence currents and the current reference limit function are adopted. In addition, a universal voltage sag generator for the various grid codes with six parameters is proposed for the verification of the LVRT performance. In order to simply extract the parameters from the LVRT curves, the LVRT profiles are divided into three regions according to the pu level and the elapsed time after voltage sags happen. With the developed voltage sag generator based on the transformer type, the LVRT strategy is performed for evaluating the various kinds of grid codes with the simple control scheme and the low cost. Based on the proposed PLL and experimental test bench, feasible FRT operations are experimented and applicable to the field.

This paper is organized as follows. Section II explains the LPN-PLL in detail when the grid voltage is polluted. In Section III, the LVRT algorithm is presented. This method is based on the DVCC and the over-current (OC) limit control. In Section IV, a prototype of voltage sag generator is presented and discussed. Section V is devoted to the FRT performance of the proposed PLL and LVRT control strategy under grid codes. Section VI provides the conclusions.

II. DESCRIPTION OF LPN-PLL

Fig. 1 shows a block diagram of the proposed LPN-PLL configuration. The grid voltage $v_a(t)$ including the harmonics can be described using Fourier series as follows:

$$\begin{aligned} v_a(t) &= V_m\cos(\omega t+\alpha)+\sum_{n=2}^{\infty}V_{mn}\cos(n\omega t+\alpha_n)\\ &\quad+\sum_{n=2}^{\infty}V_{mn}\sin(n\omega t+\alpha_n)\\ &= V_m\cos(\omega t+\alpha)+\text{Harmonics} \end{aligned} \tag{1}$$

where V_m and V_{mn} are the magnitude of the fundamental and the nth harmonics of the grid voltage, respectively, and α and α_n are the phases of the fundamental and the nth harmonics, respectively. At the beginning of the PLL process, the precise frequency of the grid voltage needs to be calculated to obtain the cosine and sine reference signals. Therefore, an accurate detection of the grid frequency is important, and this is also involved in the adaptation to the frequency variation [35]. Several techniques to obtain the frequency based on the zero-crossing detection (ZCD) [35], [36], PLL [37], Kalman filter [10], and Fourier transform [11] are available. Among those methods, ZCD method is adopted to generate the square waveforms of each phase. In order to obtain the accurate frequency of grid voltage, the low-pass filter is applied to the measured grid voltage for removing the harmonics. Although a phase delay of the grid voltage occurs, the frequency information is unaffected by the phase delay.

The reference signals $\cos(\omega t)$ and $\sin(\omega t)$ are generated by the grid frequency obtained from the frequency detector. The following equations are derived by multiplying the grid voltage with the reference signals:

$$\begin{aligned} v_{\mathrm{GridCos}}(t) =\ & v_a(t) \cdot \cos(\omega t) \\ =\ & [V_m \cos(\omega t + \alpha) + \text{harmonics}] \cdot \cos(\omega t) \\ =\ & \left[\frac{V_m \cos(\alpha) + V_m \cos(2\omega t + \alpha)}{2}\right] \\ & + \text{harmonics} \cdot \cos(\omega t) \\ v_{\mathrm{GridSin}}(t) =\ & v_a(t) \cdot \sin(\omega t) \\ =\ & [V_m \cos(\omega t + \alpha) + \text{harmonics}] \cdot \sin(\omega t) \\ =\ & \left[\frac{V_m \sin(\alpha) + V_m \sin(2\omega t + \alpha)}{2}\right] \\ & + \text{harmonics} \cdot \sin(\omega t). \end{aligned} \tag{2}$$

In order to remove $2\omega t + \alpha$ and harmonics terms of $v_{\mathrm{GridCos}}(t)$ and $v_{\mathrm{GridSin}}(t)$, fourth-order LPN filters are adopted instead of moving averaging functions [38]. From the remaining $V_m \cos(\alpha)$ and $V_m \sin(\alpha)$, the instantaneous position of the grid voltage is calculated at every sampling point as follows:

$$\begin{aligned} \alpha =\ & \tan^{-1}\left(\frac{V_m \cos(\alpha)}{V_m \sin(\alpha)}\right) \\ \theta_g =\ & \omega t + \alpha. \end{aligned} \tag{3}$$

The calculated α is the phase difference between the grid voltage (i.e., the phase of the grid voltage is $\omega t + \alpha$) and the reference signals (i.e., the phase of the reference signals is ωt).

The transfer function of the fourth-order LPN filter can be represented as a cascade realization form of the second-order factors with a real-valued coefficient

$$\begin{aligned} H_{\mathrm{LPN}}(z) =\ & H_L(z) \cdot H_N(z) \\ =\ & \left(\frac{b_{L0} + b_{L1} z^{-1} + b_{L2} z^{-2}}{1 + a_{L1} z^{-1} + a_{L2} z^{-2}}\right) \\ & \cdot \left(\frac{b_{N0} + b_{N1} z^{-1} + b_{N2} z^{-2}}{1 + a_{N1} z^{-1} + a_{N2} z^{-2}}\right). \end{aligned} \tag{4}$$

The coefficients of the LPN filter are adaptively calculated according to the grid frequency, and these are described in Table I, where T_s is the sampling period, ω_0 is the cutoff frequency, and Q is the quality factor. To eliminate the second harmonics of $v_{\mathrm{GridCos}}(t)$ and $v_{\mathrm{GridSin}}(t)$ in (2), the cutoff frequency of the notch filter should be two times of the grid frequency. To remove the remaining harmonics, the cutoff frequency $\omega_{0,lp}$ of the low-pass filter is adjustable. The lower the $\omega_{0,lp}$ is, the slower the transient response of the LPN-PLL is. For example, when the $\omega_{0,lp}$ is chosen to 60 Hz, a grid period T_g is required to obtain the valid phase angle information from the grid voltage. In contrast, when the $\omega_{0,lp}$ is increased, the steady-state accuracy cannot be guaranteed. Therefore, the ω_0 of the LPN filter is set to 120 Hz. Similarly, Q is also related to the transient response of the LPN filter. The lower the Q is, the slower the transient response of the LPN-PLL is. Q is selected as 0.625, which is a compromise between Bessel ($Q = 0.577$) and Butterworth ($Q = 0.707$).

TABLE I
COEFFICIENTS OF LPN FILTER

Coefficients for Low Pass	Equations	Coefficients for Notch	Equations
a_{L1}	$-(8Q - 2A)/C$	a_{N1}	a_{L1}
a_{L2}	$(A - B + 4Q)/C$	a_{N2}	a_{L2}
b_{L0}	A/C	b_{N0}	$(A + 4Q)/C$
b_{L1}	$2b_{L0}$	b_{N1}	a_{L1}
b_{L2}	b_{L0}	b_{N2}	b_{N0}

where $A = Q \cdot T_s^2 \cdot \omega_0^2$, $B = 2 \cdot T_s \cdot \omega_0$, $C = A + B + 4 \cdot Q$.

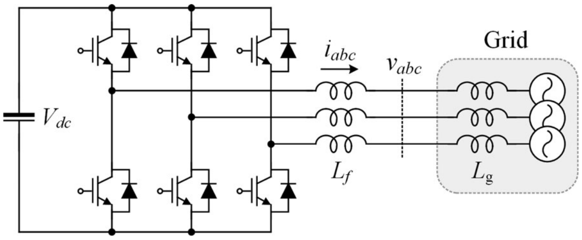

Fig. 2. Three-phase voltage source inverter connected to the grid.

III. LVRT CONTROL STRATEGY

The DG systems have to be capable to participate in full dynamic network support during grid faults (i.e., to stay connected to the network and provide voltage support by injecting a reactive current into the grid). In this section, based on the phase angle obtained from the LPN-PLL to support the stable performance in voltage sags, the LVRT control strategy is accurately described.

A. Current Reference Calculations

The LVRT performance should consider various types of voltage sags, including unbalanced conditions [39]–[41]. To follow the LVRT requirements, the grid-connected inverter needs to inject the active and required reactive currents composed of both the positive- and negative-sequence components in unbalanced voltage sags. Fig. 2 shows the three-phase voltage source inverter with the connection of the grid. In this paper, the dc-link voltage of the voltage source inverter is assumed to be constant under the LVRT operations, and supported by a dc source [4], [42].

The apparent power delivered to the grid under unbalanced conditions is expressed in the terms of the positive- and negative-sequence components [29]

$$\begin{aligned} S =\ & \left(e^{j\omega t} v_{dq}^{+} + e^{-j\omega t} v_{dq}^{-}\right)\left(e^{j\omega t} i_{dq}^{+} + e^{-j\omega t} i_{dq}^{-}\right)^{*} \\ =\ & P + jQ. \end{aligned} \tag{5}$$

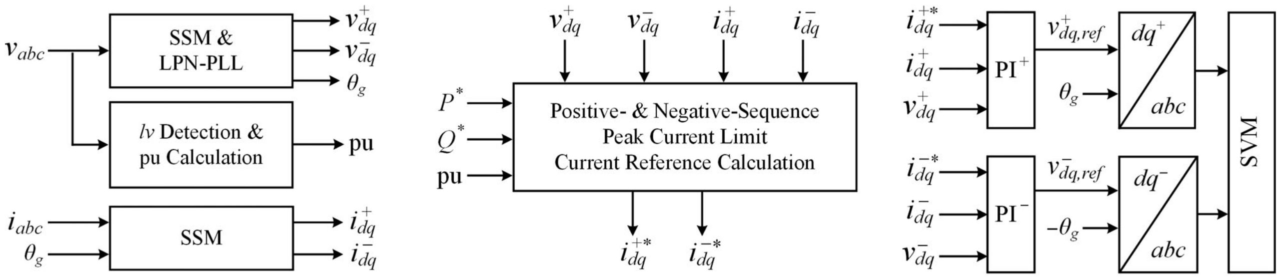

(a) (b) (c)

Fig. 3. Specified control flow for the LVRT operation. (a) Stage 1 of the LVRT operation. (b) Stage 2. (c) Stage 3.

Also, the apparent power is divided into the active power $P(t)$ and the reactive power $Q(t)$

$$P(t) = P_0 + P_{c2}\cos(2\omega t) + P_{s2}\sin(2\omega t) \tag{6}$$

$$Q(t) = Q_0 + Q_{c2}\cos(2\omega t) + Q_{s2}\sin(2\omega t) \tag{7}$$

where

$$\begin{aligned}
P_0 &= 1.5\left(v_d^+ i_d^+ + v_q^+ i_q^+ + v_d^- i_d^- + v_q^- i_q^-\right)\\
P_{c2} &= 1.5\left(v_d^+ i_d^- + v_q^+ i_q^- + v_d^- i_d^+ + v_q^- i_q^+\right)\\
P_{s2} &= 1.5\left(v_q^- i_d^+ - v_d^- i_q^+ - v_q^+ i_d^- + v_d^+ i_q^-\right)\\
Q_0 &= 1.5\left(v_q^+ i_d^+ - v_d^+ i_q^+ + v_q^- i_d^- - v_d^- i_q^-\right)\\
Q_{c2} &= 1.5\left(v_q^+ i_d^- - v_d^+ i_q^- + v_q^- i_d^+ - v_d^- i_q^+\right)\\
Q_{s2} &= 1.5\left(v_d^+ i_d^- + v_q^+ i_q^- - v_d^- i_d^+ - v_q^- i_q^+\right).
\end{aligned}$$

Due to the unbalanced grid voltage, the active power fluctuates, that is, 120 Hz ripple appears in 60 Hz power grid system. These are the second and third terms in (6) (i.e., $P_{c2}\cos(2\omega t)$ and $P_{s2}\sin(2\omega t)$), and need to be controlled to zero to remove the active power fluctuation. The reactive power fluctuation is not considered. With these assumptions about the power fluctuation, (6) and (7) can be modified to the matrix form as follows:

$$\begin{bmatrix} P_0 \\ Q_0 \\ P_{s2} \\ P_{c2} \end{bmatrix} = \frac{3}{2}\begin{bmatrix} v_d^+ & v_q^+ & v_d^- & v_q^- \\ v_q^+ & -v_d^+ & v_q^- & -v_d^- \\ v_q^- & -v_d^- & -v_q^+ & v_d^+ \\ v_d^- & v_q^- & v_d^+ & v_q^+ \end{bmatrix}\begin{bmatrix} i_d^+ \\ i_q^+ \\ i_d^- \\ i_q^- \end{bmatrix}. \tag{8}$$

From (8), current references i_d^{+*}, i_q^{+*}, i_d^{-*}, and i_q^{-*} for positive- and negative-sequence components can be obtained with the power references P^* and Q^* determined by the TSO or grid codes. P_{s2} and P_{c2} are set to zero to remove the active power fluctuation

$$\begin{aligned}
\begin{bmatrix} i_d^{+*} \\ i_q^{+*} \\ i_d^{-*} \\ i_q^{-*} \end{bmatrix} &= \frac{2}{3}\begin{bmatrix} v_d^+ & v_q^+ & v_d^- & v_q^- \\ v_q^+ & -v_d^+ & v_q^- & -v_d^- \\ v_q^- & -v_d^- & -v_q^+ & v_d^+ \\ v_d^- & v_q^- & v_d^+ & v_q^+ \end{bmatrix}^{-1}\begin{bmatrix} P^* \\ Q^* \\ 0 \\ 0 \end{bmatrix}\\
&= \frac{2P^*}{3X}\begin{bmatrix} v_d^+ \\ v_q^+ \\ -v_d^- \\ -v_q^- \end{bmatrix} + \frac{2Q^*}{3Y}\begin{bmatrix} v_q^+ \\ -v_d^+ \\ v_q^- \\ -v_d^- \end{bmatrix}
\end{aligned} \tag{9}$$

where

$$\begin{aligned}
&X \equiv \left[\left((v_d^+)^2 + (v_q^+)^2\right) - \left((v_d^-)^2 + (v_q^-)^2\right)\right]\\
&(X \neq 0 \text{ is assumed})\\
&Y \equiv \left[\left((v_d^+)^2 + (v_q^+)^2\right) + \left((v_d^-)^2 + (v_q^-)^2\right)\right]\\
&(Y \neq 0 \text{ is assumed}).
\end{aligned}$$

Equation (9) means that negative-sequence current naturally flows if grid voltage includes a negative-sequence component. In other words, due to the unbalanced grid voltage, separated current controllers are required to control positive- and negative-sequence currents for the desired active and reactive power injections.

B. Specification of LVRT Control Schemes

During the LVRT operation, the powers produced by distributed energy resource need to be reduced so that the grid-connected inverter can utilize its capacity to perform its LVRT function. For example, in WTGSs, blade pitch control, energy storage devices, and active crowbars have been researched to deal with the output power of the wind turbine during LVRT situations [34], [43], [44]. The generator-side converter controls the generator torque and pitch angles to run away from the impact of voltage sags. The generator-side converter is also controlled to balance the power flow of back-to-back (BTB) converter by a feedforward controller. And then, the grid-connected inverter supports the reactive power for the grid by calculating new references for the current controllers. In this paper, the dc-link voltage of the grid-connected inverter is supported by a dc source. Therefore, the dc-link voltage is assumed to be constant both in steady-state and under grid fault conditions, resulting in decoupling between generator- and grid-side operations. Consequently, only the grid-connected inverter is scrutinized. The LVRT control scheme is based on the LPN-PLL, the DVCC, and the peak current limitation for the fulfillment of LVRT requirements. The overall flow of the control strategy under the LVRT

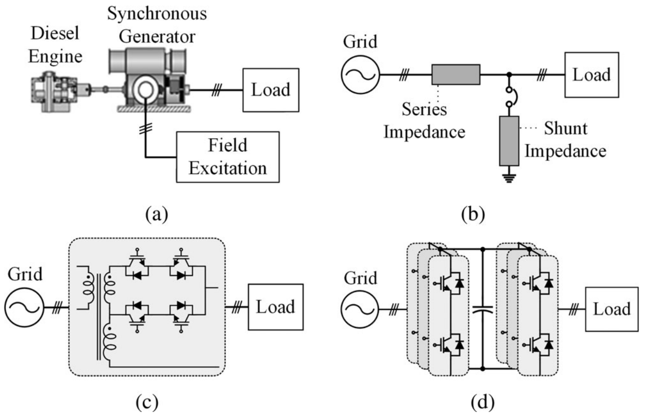

(a) (b) (c) (d)

Fig. 4. Four different types of voltage sag generators. (a) Synchronous generator-based, (b) shunt impedance-based, (c) transformer-based, and (d) BTB converter-based voltage sag generators.

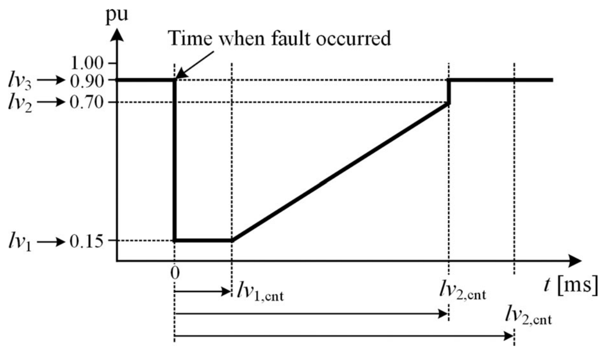

Fig. 5. Simplification of LVRT curve for extracting sag parameters.

TABLE II
PARAMETERS OF LVRT CURVES

Country	Voltage (%)			Time (ms)		
	lv_1	lv_2	lv_3	$lv_{1,\mathrm{cnt}}$	$lv_{2,\mathrm{cnt}}$	$lv_{3,\mathrm{cnt}}$
Ireland / Canada	15	90	90	625	3000	-
Italy	20	75	90	500	800	2000
Germany	0	70	90	150	750	1500
Denmark	25	75	75	150	750	-
Spain	20	80	95	500	1000	15000
User Setting	20	100	100	300	300	600

TABLE III
SPECIFICATIONS OF PROTOTYPE OF VOLTAGE SAG GENERATOR

Specifications	Values	
Rated Power	10	kV·A
Grid Voltage	380	V
Grid Frequency	60	Hz
Control Voltage	220	V
Voltage Variation Range	0–100	%
Voltage Variation Step	± 5	%
Response Time	< 1	Cycle
Control System	PLC	-
Communication Interface	RS232	-

operation is depicted in Fig. 3, and divided into three stages for the clarity.

In stage 1, the sequence separation method (SSM) and the detection of grid voltage level are the major process [29]. The three-phase grid voltages v_{abc} and currents i_{abc} are transformed into the positive- and negative-sequence SRFs with the phase angle θ_g of the grid voltage extracted by the proposed LPN-PLL. v_{dq}^{+} and i_{dq}^{+} represent the dq-axis voltages and currents in positive-sequence SRF. v_{dq}^{-} and i_{dq}^{-} represent the dq-axis voltages and currents in negative-sequence SRF. These are calculated by the SSM presented in [29]. The detection of the grid voltage level is performed by following equations

$$\begin{aligned} v_{ab,\mathrm{mag}} &= \sqrt{v_{ab}^2 + v_{ab,90^o}^2} \\ v_{bc,\mathrm{mag}} &= \sqrt{v_{bc}^2 + v_{bc,90^o}^2} \\ v_{ca,\mathrm{mag}} &= \sqrt{v_{ca}^2 + v_{ca,90^o}^2} \\ v_{lv,\mathrm{level}} &= \max[v_{ab,\mathrm{mag}}, v_{bc,\mathrm{mag}}, v_{ca,\mathrm{mag}}] \end{aligned} \tag{10}$$

where $v_{ab,90^o}$, $v_{bc,90^o}$, and $v_{ca,90^o}$ are obtained from v_{ab}, v_{bc}, and v_{ca} by a 90^o phase shifting function (i.e., first-order all-pass filter). As mentioned in the E.ON-Netz grid codes [5], the grid voltage level is determined by the largest value among line-to-line grid voltages at the PCC. Among the calculated magnitudes of the line-to-line voltages, a maximum value $v_{lv,\mathrm{level}}$ is selected to determine the pu level of the grid voltage.

In stage 2, the current references for the DVCC are calculated not to exceed the OC limit of the grid-connected inverter. During the normal operation, the power factor of the grid-connected inverter is controlled to unity and the average reactive power is controlled to zero. However, to meet the LVRT requirements of the grid codes when the voltage sags happen, the reactive power should be injected into the grid as follows:

$$\begin{aligned} &0.0 \le \mathrm{pu} \le 0.5 \begin{cases} P^* = 0 \\ Q^* = P_{\max} \end{cases} \\ &0.5 < \mathrm{pu} \le 0.9 \begin{cases} P^* = \sqrt{P_{\max}^2 - Q^{*2}} \\ Q^* = 2(1 - \mathrm{pu})P_{\max} \end{cases} \\ &0.9 < \mathrm{pu} \le 1.0 \begin{cases} P^* = P_{\max} \\ Q^* = 0 \end{cases} . \end{aligned} \tag{11}$$

As shown in (11), the active and reactive power references P^* and Q^* are determined according to the pu level of the grid voltage. And then, the P^* and Q^* are put into the calculation of the current references as follows:

$$\begin{aligned} i_d^{+*} &= \frac{2}{3}\left(\frac{v_d^+}{X}P^* + \frac{v_q^+}{Y}Q^*\right) \\ i_q^{+*} &= \frac{2}{3}\left(\frac{v_q^+}{X}P^* - \frac{v_d^+}{Y}Q^*\right) \\ i_d^{-*} &= \frac{2}{3}\left(-\frac{v_d^-}{X}P^* + \frac{v_q^-}{Y}Q^*\right) \\ i_q^{-*} &= \frac{2}{3}\left(-\frac{v_q^-}{X}P^* - \frac{v_d^-}{Y}Q^*\right). \end{aligned} \tag{12}$$

TABLE IV
SPECIFICATIONS OF THE THREE-PHASE VOLTAGE SOURCE INVERTER

Specifications	Values	
Rated dc-Link Voltage	600	V_{dc}
Rated Current	37	A
Rated Power	10	kW
Grid Voltage	220/380	V_{ac}
Frequency	60	Hz
Power Factor	> 0.96	-
THD	< 4.0	%
Over Load	110	%
Maximum Efficiency	95	%
Phase Current	34	A
Trans. Turn Ratio	170:380	-
Switching Frequency	7.2	kHz
Filter Inductance	3	mH

In addition, there is still one more step to obtain final current references. These current references in (12) produce negative-sequence currents to reduce the active power ripple and meet the LVRT requirements. However, this control strategy may lead to the excessively high peak current resulting in the output filter saturation or the OC condition. Consequently, the grid-connected inverter will trip from the grid and fail the LVRT performance. Therefore, the scaled new current references are required to prevent the system fail. The maximum value of the current reference $i_{\max}$ can be calculated as follows:

$$i_{\max} = \sqrt{\left(i_d^{+*}\right)^2 + \left(i_q^{+*}\right)^2 + \left(i_d^{-*}\right)^2 + \left(i_q^{-*}\right)^2}. \tag{13}$$

To limit the current references within the allowable range of hardware specification, the scaling factor f_{scale} is obtained as follows:

$$f_{\text{scale}} = \begin{cases} i_{\text{limit}}/i_{\max} & (i_{\text{limit}} < i_{\max}) \\ 1.0 & (i_{\text{limit}} \geq i_{\max}) \end{cases} \tag{14}$$

where i_{limit} is the maximum current allowed for the hardware specification. Consequently, if the calculated current references are higher than i_{limit}, the current references obtained from (12) should be scaled down as follows:

$$\begin{aligned} i_{d,\text{scaled}}^{+*} &= i_d^{+*} \cdot f_{\text{scale}} \\ i_{q,\text{scaled}}^{+*} &= i_q^{+*} \cdot f_{\text{scale}} \\ i_{d,\text{scaled}}^{-*} &= i_d^{-*} \cdot f_{\text{scale}} \\ i_{q,\text{scaled}}^{-*} &= i_q^{-*} \cdot f_{\text{scale}}. \end{aligned} \tag{15}$$

In stage 3, the voltage references for the space-vector modulation (SVM) are generated through the DVCC. The dq-axis currents in individual positive- and negative-sequence SRFs are controlled by PI controllers and their outputs are added. Finally, these are converted into switching signals by the SVM.

IV. IMPLEMENTATION OF TRANSFORMER-BASED VOLTAGE SAG GENERATOR

To evaluate the LVRT performance of the grid-connected inverter, a voltage sag generator is essential at the final stage of development. There are four types of voltage sag generators as shown in Fig. 4.

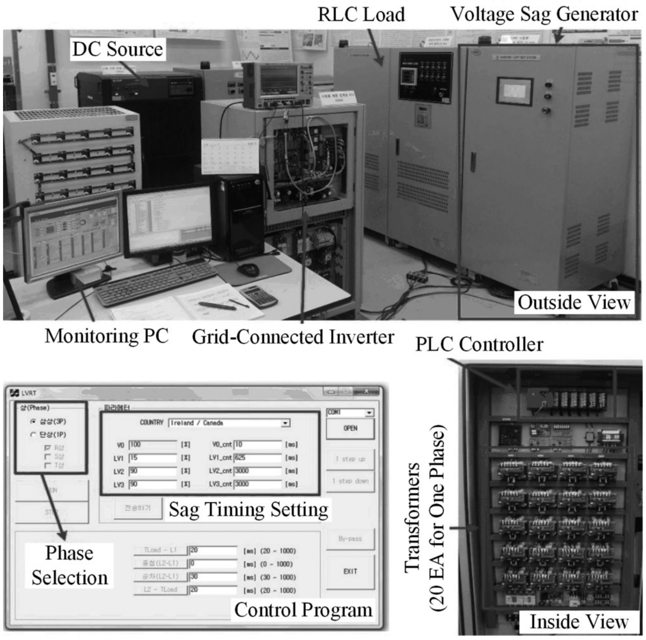

상(Phase)
● 삼상(3P)
○ 단상(1P)
☑ R상
☐ S상
☐ T상

파라메터
COUNTRY: Ireland / Canada
V0: 100 [%] V0_cnt: 10 [ms]
LV1: 15 [%] LV1_cnt: 625 [ms]
LV2: 90 [%] LV2_cnt: 3000 [ms]
LV3: 90 [%] LV3_cnt: 3000 [ms]

TLoad - L1: 20 [ms] (20 - 1000)
중첩(L2-L1): 0 [ms] (0 - 1000)
순차(L2-L1): 30 [ms] (30 - 1000)
L2 - TLoad: 20 [ms] (20 - 1000)

Fig. 6. Layout of the experimental setup.

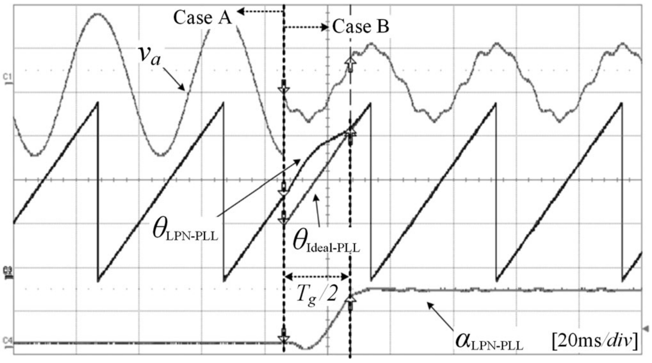

Fig. 7. Experimental results of LPN-PLL with the voltage sag, the harmonics, and the phase jump. Grid voltage v_a, $\theta_{\text{Ideal-PLL}}$, $\theta_{\text{LPN-PLL}}$ (in radians), and $\alpha_{\text{LPN-PLL}}$ (in radians) are measured.

These are synchronous generator-based [45], shunt impedance-based [46], [47], transformer-based [48]–[50], and BTB converter-based [51]–[53] voltage sag generators. In the case of the synchronous generator-based voltage sag generator, the cost of the hardware system is considerably high, and only balanced voltage sags are generated. The shunt impedance-based voltage sag generator can control balanced or unbalanced voltage sags with the combination of the reactors and series-connected bidirectional power switches. However, the rating of fault currents through the path of the shunt impedances is somewhat high. The BTB converter is a very powerful solution to generate most kinds of grid faults. However, the cost of the BTB converter hardware is high, and the software for the control algorithm is more complex than the other voltage sag generators. Therefore, in this paper, the transformer-based

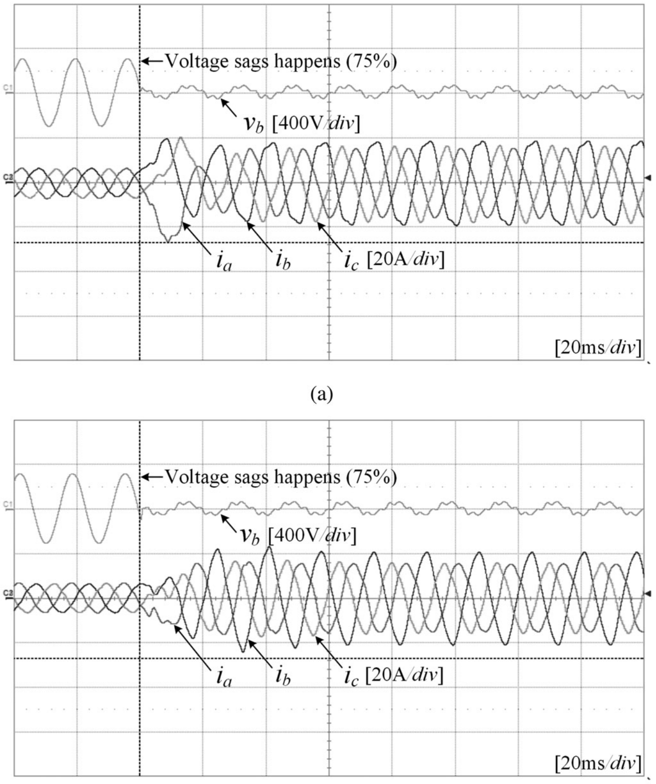

(a)

(b)

Fig. 8. Experimental results for comparison between the conventional PLL and the proposed PLL under unbalanced 75% voltage sag. (a) Conventional PLL (SRF-PLL). (b) Proposed PLL (LPN-PLL).

voltage sag generator is adopted for the evaluation of the LVRT performance, and this is controlled by the programmable logic controller (PLC). With this solution, the prototype of the voltage sag generator can generate various kinds of grid codes with the simple control scheme and the low cost.

The prototype of 10 kV·A voltage sag generator is composed of step transformers (20 EA for the one phase) and bidirectional power switches (Triac or Thyristor). The single transformer takes 5% of voltage sags or variations. Furthermore, the prototype can generate the balanced or unbalanced voltage sags, including voltage profiles according to the LVRT curves of the grid codes. To simplify and extract the parameters from the LVRT curves, the LVRT profiles are divided into three regions according to the pu levels and the elapsed times after the grid fault happens as shown in Fig. 5. The extracted parameters of representative grid codes are summarized in Table II.

With these parameters, the PLC unit controls the bidirectional power switches to generate the voltage sags. The user can put the parameters arbitrarily or select the country through the control program, which is installed in the panel computer for the prototype. The control program for the voltage sag generator is designed with the microsoft foundation class and interfaced with the PLC unit through the RS-232 communication. Specifications of the prototype of the voltage sag generator are shown in Table III.

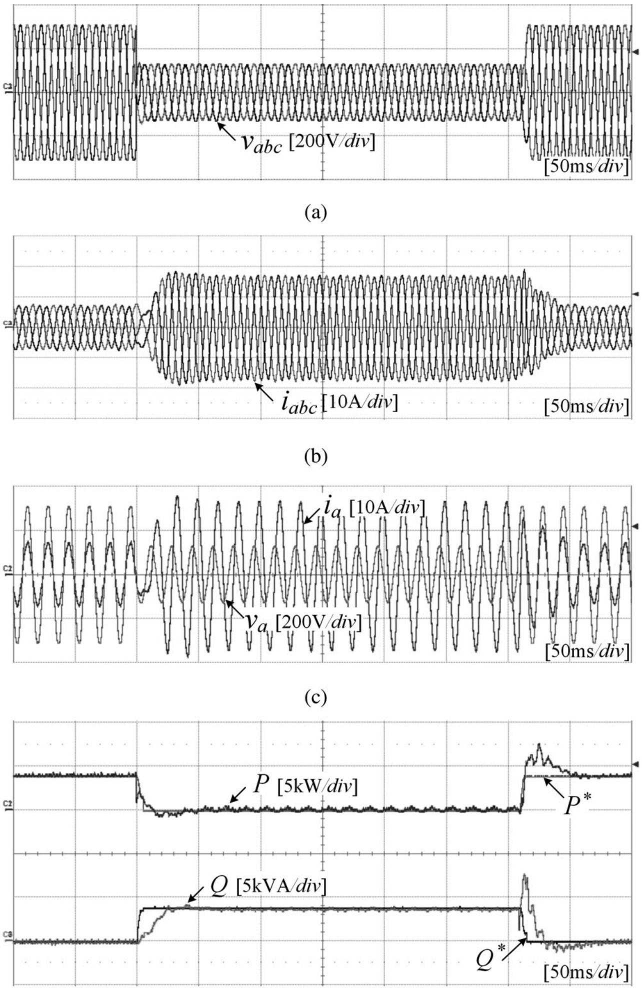

(d)

Fig. 9. Experimental results of the LVRT performance under balanced 60% voltage sag (Type A). (a) Grid voltages. (b) Grid currents. (c) Grid voltage and current in phase A. (d) Instantaneous active and reactive powers and their references.

V. EXPERIMENTAL VERIFICATIONS

In this paper, the proposed LVRT techniques based on LPN-PLL are evaluated by using an experimental setup controlled by a Texas Instruments floating point DSP TMS320F28335. The specifications of 10 kW three-phase voltage source inverter are summarized in Table IV. Fig. 6 shows the laboratory environment for evaluating the grid-connected inverter with the voltage sag generator. A 33 kW passive (*RLC*) load is connected in shunt between the inverter and the grid. The voltage sag generator is connected in series between the inverter and the grid. The purpose is to assess the performance of the grid-connected inverter during LVRT operation based on the phase angle obtained from the LPN-PLL.

A. LVRT Performance Comparison With Different PLLs

The representative experimental result of LPN-PLL is described in this section.

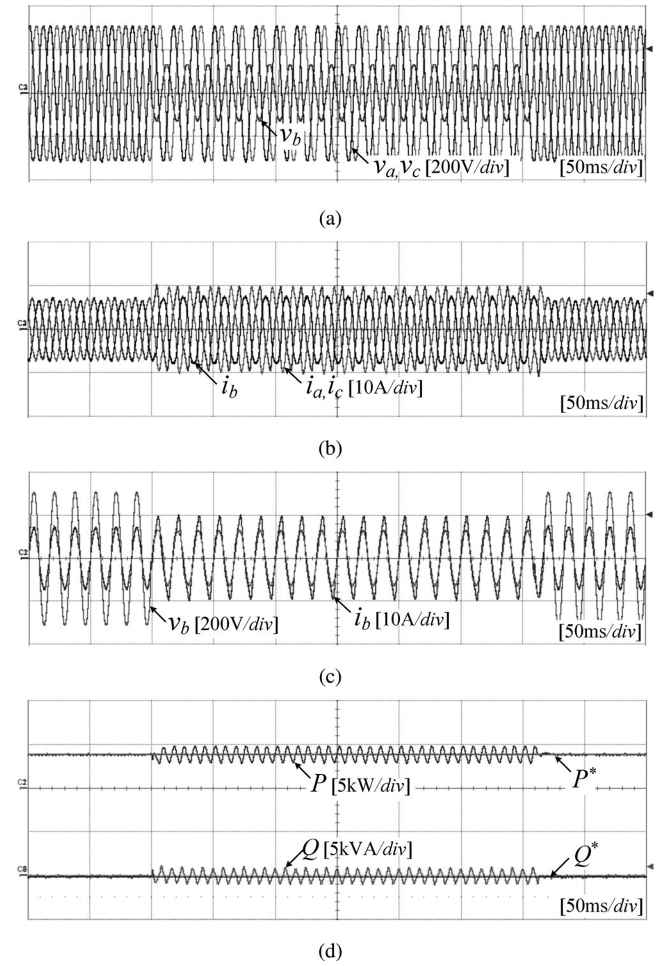

Fig. 10. Experimental results of the LVRT performance under unbalanced 60% sag without DVCC (Type B, only the voltage sag in phase B happens). (a) Grid voltages. (b) Grid currents. (c) Grid voltage and current in phase B. (d) Instantaneous active and reactive powers and their references.

1) normal grid voltage (Case A): $v_a = v_b = v_c = 1.0$ pu, and $\theta = 0°$ (no phase jump);
2) grid voltage sag in phase A with harmonics and phase jump (Case B) : $v_{a,1} = 0.5$ pu, $v_{a,5} = 0.05$ pu, $v_{c,5} = 0.1$ pu, and $\theta = 60°$.

As shown in Fig. 7, in the case of severe conditions for the LPN-PLL (i.e., the grid voltage is distorted seriously with the voltage sag, the symmetrical harmonics, and the 60° phase jump), the estimated phase angle $\theta_{\mathrm{LPN-PLL}}$ follows the ideal phase angle $\theta_{\mathrm{Ideal-PLL}}$ within 0.5 T_g (8.33 ms).

In order to verify the improvement of the current transient response by the LPN-PLL when the unbalanced voltage sags happen, the SRF-PLL and the LPN-PLL were compared in the same condition. As shown in Fig. 8, the variations of inverter currents gradually reduced in all phases. The current transition of the SRF-PLL is rougher and the peak value of the inverter current is higher than the LPN-PLL. This result shows that the possibility to be disconnected by the current fault can be considerably reduced by only the change of the PLL method. The proposed LPN-PLL is suitable to improve the reliability of the FRT performance.

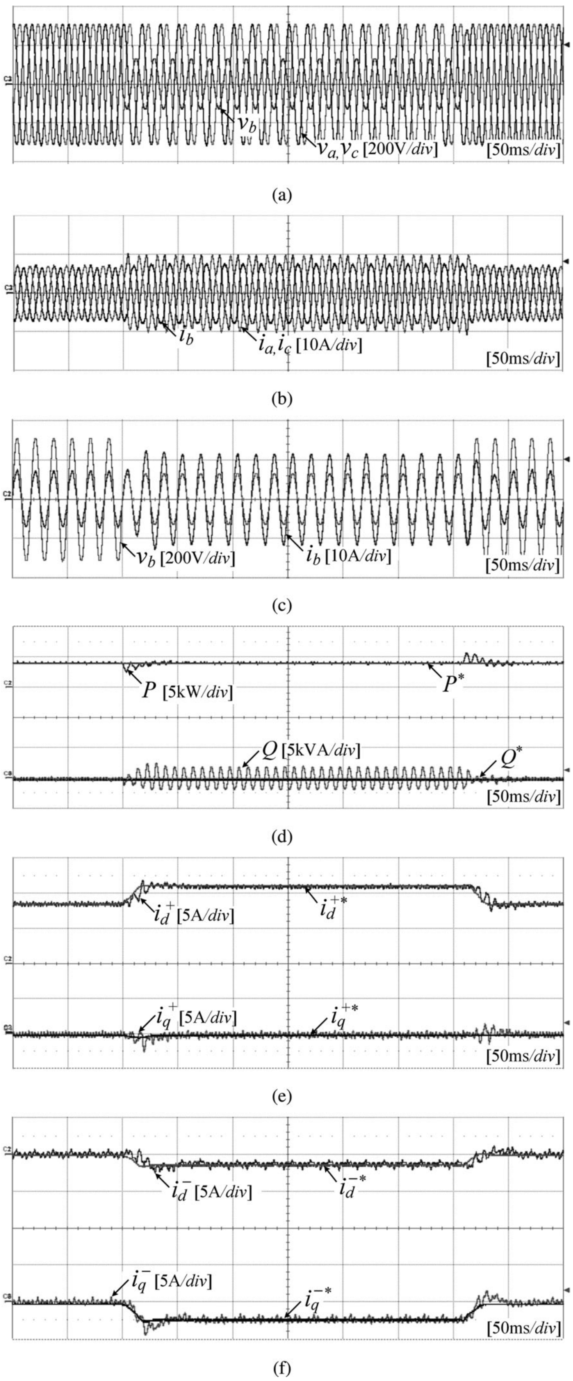

Fig. 11. Experimental results of the LVRT performance under unbalanced 60% sag with DVCC (Type B, only the voltage sag in phase B happens). (a) Grid voltages. (b) Grid currents. (c) Grid voltage and current in phase B. (d) Instantaneous active and reactive powers and their references. (e) dq-axis currents and their references of positive-sequence SRF. (f) dq-axis currents and their references of negative-sequence SRF.

B. LVRT Performance Under Balanced and Unbalanced Sags

The voltage sags are generated by the prototype of the voltage sag generator for the evaluation of the LVRT performance during 300 ms. In order to fully support the reactive power, $P_{\max}$ in (11) is chosen by the power ratings of the prototype of the grid-connected inverter. The references of active and reactive powers

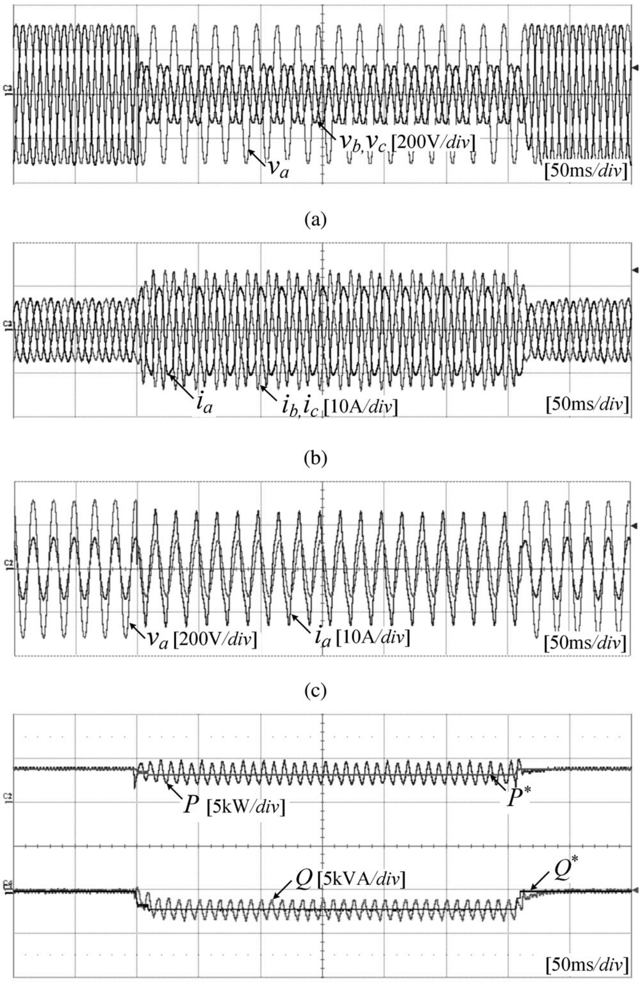

(a)

(b)

(c)

(d)

Fig. 12. Experimental results of the LVRT performance under unbalanced 60% sag without DVCC (Type E, the voltage sags in phase B and C happen). (a) Grid voltages. (b) Grid currents. (c) Grid voltage and current in phase A. (d) Instantaneous active and reactive powers and their references.

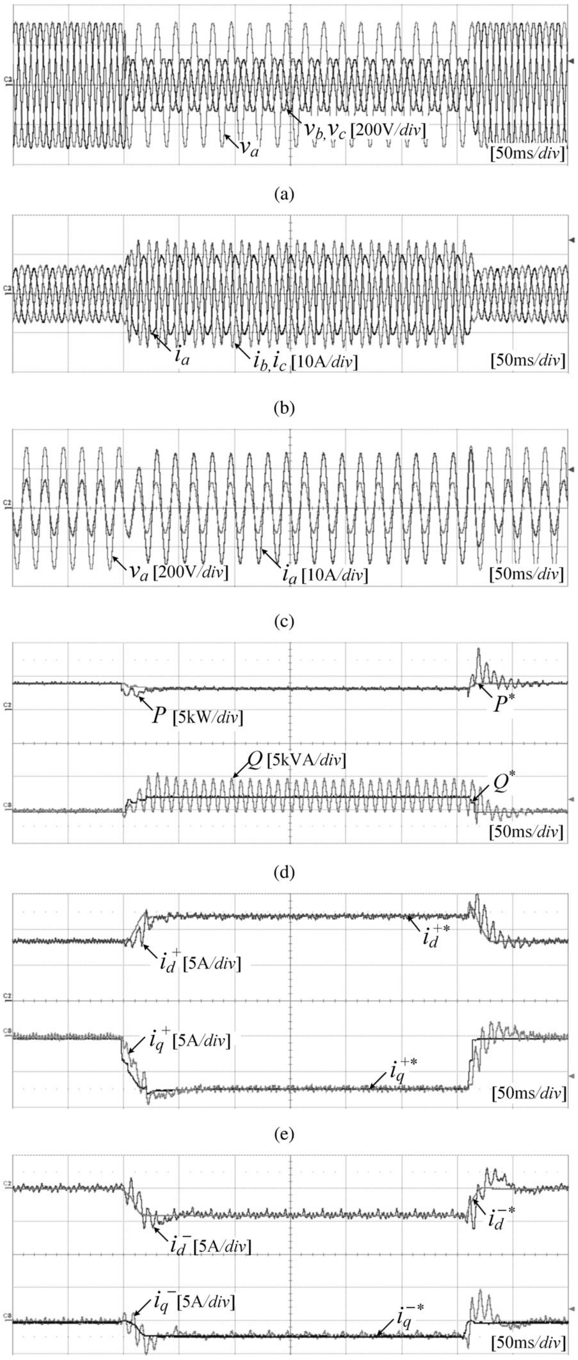

(a)

(b)

(c)

(d)

(e)

(f)

Fig. 13. Experimental results of the LVRT performance under unbalanced 60% sag with DVCC (Type E, the voltage sags in phase B and C happen). (a) Grid voltages. (b) Grid currents. (c) Grid voltage and current in phase A. (d) Instantaneous active and reactive powers and their references. (e) dq-axis currents and their references of positive-sequence SRF. (f) dq-axis currents and their references of negative-sequence SRF.

are calculated by (11) with the measured pu level to identify the degree of the voltage sags, and the references of positive- and negative-sequence dq-axis currents are calculated by (12) with the calculated power references.

Experimental results of the three-phase balanced 60% voltage sag (i.e., type A) are shown in Fig. 9. The grid voltages and currents and the instantaneous active and reactive powers P and Q with their references P^* and Q^* are represented in the experimental results. In this case, symmetrical and balanced reactive currents are injected in the grid during the voltage sags. Because the obtained pu level is below 0.5, only the reactive power is injected into the grid. Also, there is no power ripple during the LVRT operation.

Experimental results of the three-phase unbalanced 60% voltage sag for type B without the DVCC are shown in Fig. 10. Only the grid voltage in phase B is reduced to 40% of the nominal voltage. Because the detection of the pu level finds the maximum value of the line-to-line voltage, there are no variations of the power references (i.e., $P^* = P_{\max}$, $Q^* = 0$). Due to no activation of the DVCC, the power ripples appear in both the active and reactive powers. However, the average values of active and reactive powers are the same as the power references.

Experimental results of the three-phase unbalanced 60% voltage sag for type B with the DVCC are shown in Fig. 11. Compared with no activation of the DVCC [see Fig. 10], it is noticed

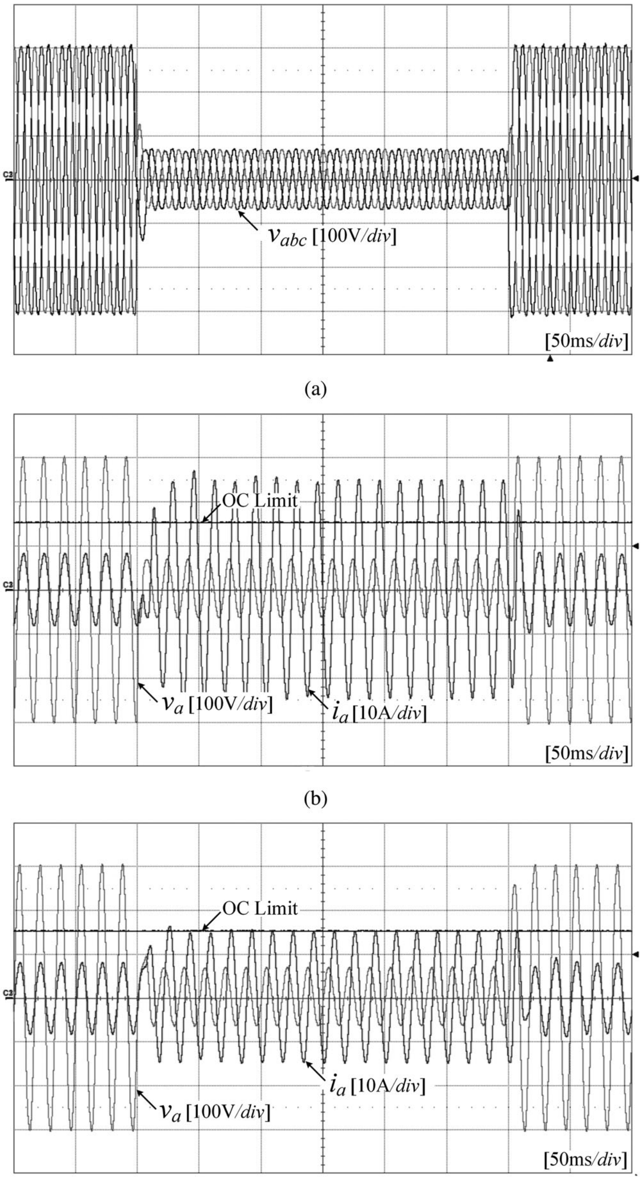

(a)

(b)

(c)

Fig. 14. Experimental results of the LVRT performance with the OC limit control. (a) Grid voltages. (b) Grid voltage and current in phase A without the OC limit control. (b) Grid voltage and current in phase A with the OC limit control.

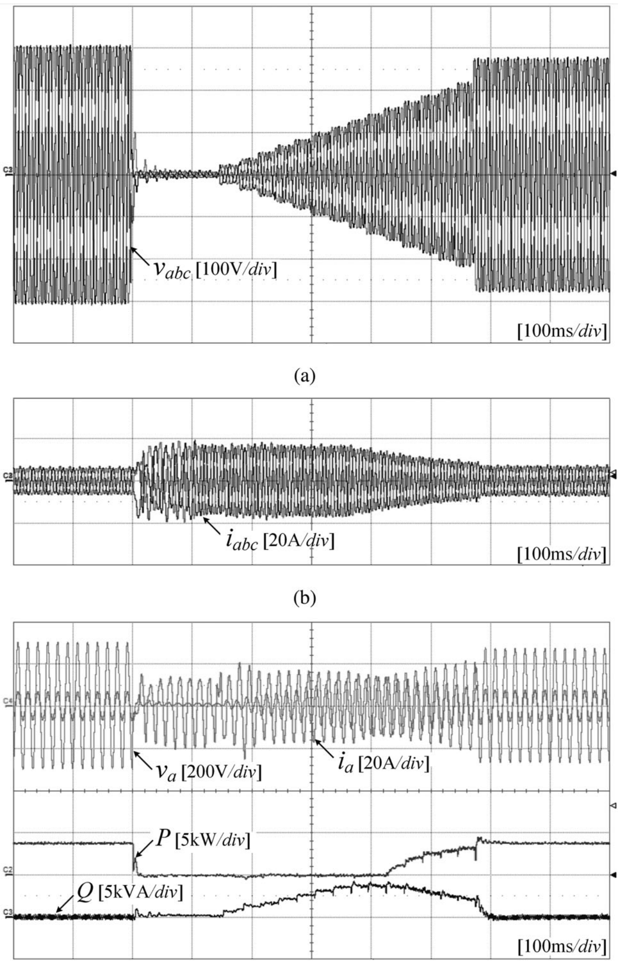

(a)

(b)

(c)

Fig. 15. Experimental results of the LVRT performance with German grid code (a) Grid voltages. (b) Grid currents. (c) Grid voltage and current in phase A, and instantaneous active and reactive powers.

that the ripple of the active power is controlled to zero. For the verification of the DVCC, the dq-axis current references in positive- and negative-sequence SRFs are represented, and it is shown that the individual currents are controlled with their references. The average value of the reactive power is controlled according to the LVRT requirements during voltage sags.

Experimental results of the three-phase unbalanced 60% voltage sag for type E without the DVCC are shown in Fig. 12. The grid voltages in phases B and C are reduced to 40% of the nominal voltages. Compared with type B, there is the decrease of the pu level of the grid voltage, and the pu level is between 0.5 and 0.9. Therefore, the active power reference is reduced, and reactive power is injected when the voltage sags happen. Also, the power ripple exists in the active power due to no activation of the DVCC.

Experimental results of the three-phase unbalanced 60% voltage sag for type E with the DVCC are shown in Fig. 13. Due to the DVCC, the active power fluctuation is removed, and the average value of the reactive power is the same as the reactive power reference. The dq-axis currents and their references in positive- and negative-sequence SRFs are represented.

C. LVRT Performance With OC Limit Control

Experimental results of the LVRT performance with the OC limit control are shown in Fig. 14. Also, the voltage sags are generated with the prototype of the voltage sag generator during 300 ms. The active power reference is set to 3 kW at the normal operation and the OC limit is set to 17 A. When 70% balanced voltage sag happens without the OC limit control, the peak current is higher than the OC limit as shown in Fig. 14(b). This leads to the system trip by the OC protection. Therefore, in order to prevent this situation, the current references should be scaled

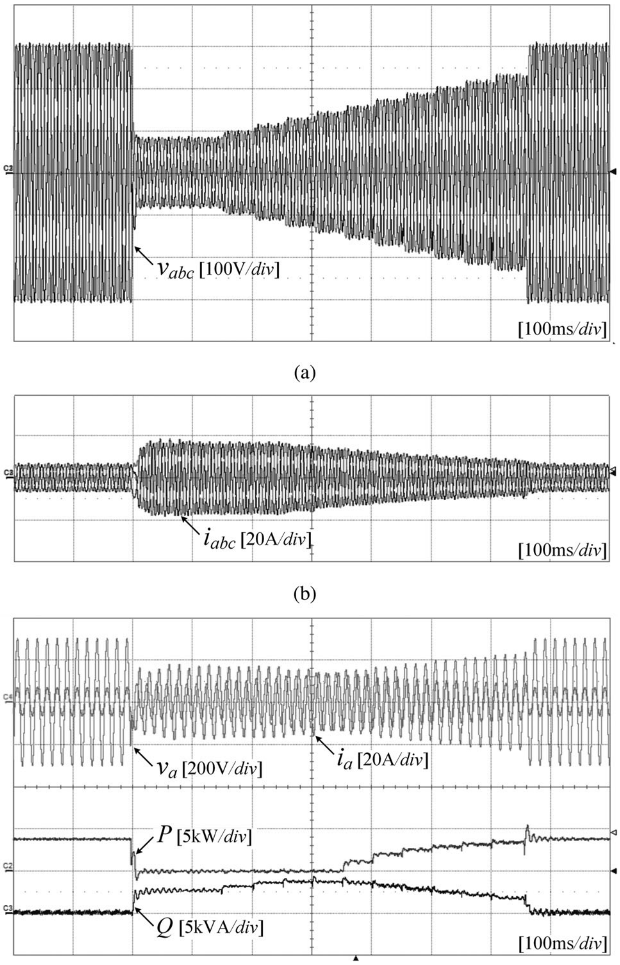

Fig. 16. Experimental results of the LVRT performance with Danish grid code. (a) Grid voltages. (b) Grid currents. (c) Grid voltage and current in phase A, and instantaneous active and reactive powers.

down. Fig. 14(c) shows that the peak current becomes lower than the OC limit by scaling down the current references with (14) and (15).

D. LVRT Performance With Various Grid Codes

The LVRT performances according to the various grid codes are verified with the prototype of the voltage sag generator. Among the grid codes, Germany, Denmark, and Canada are selected for the evaluation. The sag timing parameters were set up in the voltage sag generator with the parameters in Table II.

Fig. 15(a) shows the LVRT curve of Germany with the zero voltage period during 150 ms. As shown in Fig. 15(b), even in the zero voltage period, the grid currents are stably controlled according to the grid code. The instantaneous active and reactive powers injected into the grid is shown in Fig. 15(c). Fig. 16(a) shows the LVRT curve of Denmark with the ten steps of the LVRT from 0.25 to 0.75 pu because the voltage sags by the prototype are generated with 5% step changes. The grid-connected inverter shows good LVRT performances in Fig. 16(b) and (c).

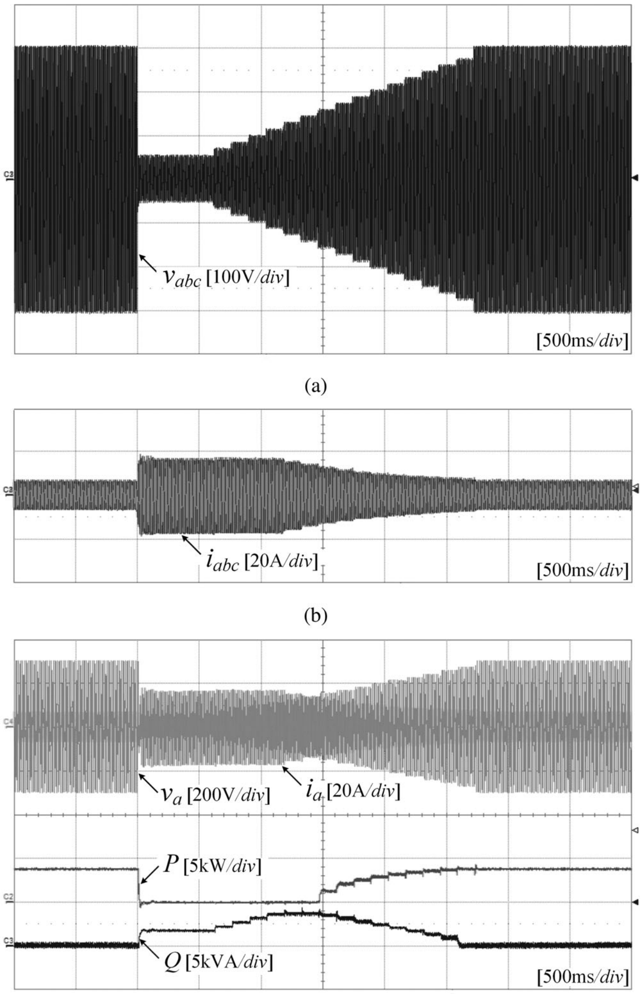

(c)

Fig. 17. Experimental results of the LVRT performance with Canadian grid code. (a) Grid voltages. (b) Grid currents. (c) Grid voltage and current in phase A, and instantaneous active and reactive powers.

The LVRT performance under Canadian grid code is represented in Fig. 17. During the voltage sags, the grid-connected inverter supports the grid by injecting the reactive power. As soon as the grid voltages recover to nominal voltages, the grid-connected inverter injects only the active power into the grid.

VI. CONCLUSION

This paper presented FRT techniques for the grid-connected inverter based on the LPN-PLL with adaptive disturbance elimination properties. The LPN-PLL could robustly reject disturbances under voltage sags, unbalance, and harmonic distortion regardless of the variations in the phase and frequency of the grid voltage. The proposed synchronization method is based on the FFT-PLL structure using the FFT concept unlike the conventional SRF-PLL method, which requires a three-phase voltage and the gain tuning of PI controller. In order to evaluate the performance of the grid-connected inverter under grid faults, the 10 kV·A transformer-based voltage sag generator was implemented, which can generate various kinds of grid codes with simple control scheme and low cost. The LVRT control strategy was described in detail. The LVRT performances of the LPN-PLL was verified by applying the detailed control schemes in a 10 kW grid-connected inverter through experimental evaluations for the various kinds of voltage sags and grid codes. The LPN-PLL behaved appropriately under a range of grid voltage faults. Also, the LVRT operation with the DVCC and the OC limit control showed excellent performances. Based on the proposed method and experimental test bench, feasible FRT operation is guaranteed and applicable to the field situation.

REFERENCES

[1] Z. Chen, J. M. Guerrero, and F. Blaabjerg, “A review of the state of the art of power electronics for wind turbines,” *IEEE Trans. Power Electron.*, vol. 24, no. 8, pp. 1859–1875, Aug. 2009.

[2] W. Sinsukthavorn, E. Ortjohann, A. Mohd, N. Hamsic, and D. Morton, “Control strategy for three-/four-wire-inverter-based distributed generation,” *IEEE Trans. Ind. Electron.*, vol. 59, no. 10, pp. 3890–3899, Oct. 2012.

[3] S. Yang, Q. Lei, F. Z. Peng, and Z. Qian, “A robust control scheme for grid-connected voltage-source inverters,” *IEEE Trans. Ind. Electron.*, vol. 58, no. 1, pp. 202–212, Jan. 2011.

[4] C.-T. Lee, C.-W. Hsu, and P.-T. Cheng, “A low-voltage ride-through technique for grid-connected converters of distributed energy resources,” *IEEE Trans. Ind. Appl.*, vol. 47, no. 4, pp. 1821–1832, Jul./Aug. 2011.

[5] *Grid Code: High and Extra High Voltage*, E.ON Netz GmbH, Bayreuth, Germany, 2006.

[6] J. Miret, A. Camacho, M. Castilla, L. G. de Vicuna, and J. Matas, “Control scheme with voltage support capability for distributed generation inverters under voltage sags,” *IEEE Trans. Power Electron.*, vol. 28, no. 11, pp. 5252–5262, Nov. 2013.

[7] J. P. da Costa, H. Pinheiro, T. Degner, and G. Arnold, “Robust controller for DFIGS of grid-connected wind turbines,” *IEEE Trans. Ind. Electron.*, vol. 58, no. 9, pp. 4023–4038, Sep. 2011.

[8] D. Xiang, L. Ran, P. J. Tavner, and S. Yang, “Control of a doubly fed induction generator in a wind turbine during grid fault ride-through,” *IEEE Trans. Energy Convers.*, vol. 21, no. 3, pp. 652–662, Sep. 2006.

[9] J. Morren and S. W. H. de Haan, “Ridethrough of wind turbines with doubly-fed induction generator during a voltage dip,” *IEEE Trans. Energy Convers.*, vol. 20, no. 2, pp. 435–441, Jun. 2005.

[10] G.-C. Hsieh and J. C. Hung, “Phase-locked loop techniques. A survey,” *IEEE Trans. Ind. Electron.*, vol. 43, no. 6, pp. 609–615, Dec. 1996.

[11] M. Kesler and E. Ozdemir, “Synchronous-reference-frame-based control method for UPQC under unbalanced and distorted load conditions,” *IEEE Trans. Ind. Electron.*, vol. 58, no. 9, pp. 3967–3975, Sep. 2011.

[12] G. Escobar, M. F. Martinez-Montejano, A. A. Valdez, P. R. Martinez, and M. Hernandez-Gomez, “Fixed-reference-frame phase-locked loop for grid synchronization under unbalanced operation,” *IEEE Trans. Ind. Electron.*, vol. 58, no. 5, pp. 1943–1951, May 2011.

[13] J. P. Lee, B. D. Min, T. J. Kim, D. W. Yoo, and J. Y. Yoo, “Active frequency with a positive feedback anti-islanding method based on a robust PLL algorithm for grid-connected PV PCS,” *J. Power Electron.*, vol. 11, no. 3, pp. 360–368, May 2011.

[14] M. Karimi-Ghartemani and M. R. Iravani, “A method for synchronization of power electronic converters in polluted and variable-frequency environments,” *IEEE Trans. Power Syst.*, vol. 19, no. 3, pp. 1263–1270, Aug. 2004.

[15] C. H. da Silva, R. R. Pereira, L. E. B. da Silva, G. Lambert-Torres, B. K. Bose, and S. U. Ahn, “A digital PLL scheme for three-phase system using modified synchronous reference frame,” *IEEE Trans. Ind. Electron.*, vol. 57, no. 11, pp. 3814–3821, Nov. 2010.

[16] P. Rodriguez, L. Sainz, and J. Bergas, “Synchronous double reference frame PLL applied to a unified power quality conditioner,” in *Proc. 10th Int. Conf. Harmonics Quality Power*, Oct. 6–9, 2002, vol. 2, pp. 614–619.

[17] P. Rodriguez, J. Pou, J. Bergas, I. Candela, R. Burgos, and D. Boroyevich, “Double synchronous reference frame PLL for power converters control,” in *Proc. IEEE 36th Power Electron. Spec. Conf.*, Jun. 16, 2005, pp. 1415–1421.

[18] R. I. Bojoi, G. Griva, V. Bostan, M. Guerriero, F. Farina, and F. Profumo, “Current control strategy for power conditioners using sinusoidal signal integrators in synchronous reference frame,” *IEEE Trans. Power Electron.*, vol. 20, no. 6, pp. 1402–1412, Nov. 2005.

[19] P. Rodriguez, R. Teodorescu, I. Candela, A. V. Timbus, M. Liserre, and F. Blaabjerg, “New positive-sequence voltage detector for grid synchronization of power converters under faulty grid conditions,” in *Proc. IEEE 37th Power Electron. Spec. Conf.*, Jun. 18–22, 2006, pp. 1–7.

[20] P. Rodriguez, J. Pou, J. Bergas, J. I. Candela, R. P. Burgos, and D. Boroyevich, “Decoupled double synchronous reference frame PLL for power converters control,” *IEEE Trans. Power Electron.*, vol. 22, no. 2, pp. 584–592, Mar. 2007.

[21] F. A. S. Neves, M. C. Cavalcanti, H. E. P. de Souza, E. J. Bueno, and M. Rizo, “A generalized delayed signal cancellation method for detecting fundamental-frequency positive-sequence three-phase signals,” *IEEE Trans. Power Del.*, vol. 25, no. 3, pp. 1816–1825, Jul. 2010.

[22] F. A. S. Neves, H. E. P. de Souza, M. C. Cavalcanti, F. Bradaschia, and E. J. Bueno, “Digital filters for fast harmonic sequence component separation of unbalanced and distorted three-phase signals,” *IEEE Trans. Ind. Electron.*, vol. 59, no. 10, pp. 3847–3859, Oct. 2012.

[23] Y. F. Wang and Y. W. Li, “Three-phase cascaded delayed signal cancellation PLL for fast selective harmonic detection,” *IEEE Trans. Ind. Electron.*, vol. 60, no. 4, pp. 1452–1463, Apr. 2013.

[24] *IEEE Standard for Interconnecting Distributed Resources With Electric Power Systems*, IEEE Standard 1547-2003, Jul. 2003.

[25] R. Pena, R. Cardenas, J. Proboste, G. Asher, and J. Clare, “Sensorless control of doubly-fed induction generators using a rotor-current-based MRAS observer,” *IEEE Trans. Ind. Electron.*, vol. 55, no. 1, pp. 330–339, Jan. 2008.

[26] S. M. A. Cruz, A. Stefani, F. Filippetti, and A. J. M. Cardoso, “A new model-based technique for the diagnosis of rotor faults in RFOC induction motor drives,” *IEEE Trans. Ind. Electron.*, vol. 55, no. 12, pp. 4218–4228, Dec. 2008.

[27] A. K. Jain and V. T. Ranganathan, “Wound rotor induction generator with sensorless control and integrated active filter for feeding nonlinear loads in a stand-alone grid,” *IEEE Trans. Ind. Electron.*, vol. 55, no. 1, pp. 218–228, Jan. 2008.

[28] Z. Qingrong and C. Liuchen, “An advanced SVPWM-based predictive current controller for three-phase inverters in distributed generation systems,” *IEEE Trans. Ind. Electron.*, vol. 55, no. 3, pp. 1235–1246, Mar. 2008.

[29] S. Alepuz, S. Busquets-Monge, J. Bordonau, J. A. Martinez-Velasco, C. A. Silva, J. Pontt, and J. Rodriguez, “Control strategies based on symmetrical components for grid-connected converters under voltage dips,” *IEEE Trans. Ind. Electron.*, vol. 56, no. 6, pp. 2162–2173, Jun. 2009.

[30] S. Alepuz, A. Calle, S. Busquets-Monge, S. Kouro, and B. Wu, “Use of stored energy in PMSG rotor inertia for low-voltage ride-through in back-to-back NPC converter-based wind power systems,” *IEEE Trans. Ind. Electron.*, vol. 60, no. 5, pp. 1787–1796, May 2013.

[31] K.-H. Kim, Y.-C. Jeung, D.-C. Lee, and H.-G. Kim, “LVRT scheme of PMSG wind power systems based on feedback linearization,” *IEEE Trans. Ind. Electron.*, vol. 27, no. 5, pp. 2376–2384, May 2012.

[32] H. Geng, C. Liu, and G. Yang, “LVRT capability of DFIG-based WECS under asymmetrical grid fault condition,” *IEEE Trans. Ind. Electron.*, vol. 60, no. 6, pp. 2495–2509, Jun. 2013.

[33] K. Ma, M. Liserre, and F. Blaabjerg, “Operating and loading conditions of a three-level neutral-point-clamped wind power converter under various grid faults,” *IEEE Trans. Ind. Appl.*, vol. 50, no. 1, pp. 520–530, Jan./Feb. 2014.

[34] M. Rizo, A. Rodriguez, E. Bueno, F. J. Rodriguez, and C. Giro, “Low voltage ride-through of wind turbine based on interior permanent magnet synchronous generators sensorless vector controlled,” in *Proc. IEEE Energy Convers. Congr. Expo.*, Sep. 12–16, 2010, pp. 2507–2514.

[35] J.-P. Lee, B.-D. Min, T.-J. Kim, D.-W. Yoo, and J.-Y. Yoo, “A novel topology for photovoltaic dc/dc full-bridge converter with flat efficiency under wide PV module voltage and load range,” *IEEE Trans. Ind. Electron.*, vol. 55, no. 7, pp. 2655–2663, Jul. 2008.

[36] B.-D. Min, J.-P. Lee, J.-H. Kim, T.-J. Kim, D.-W. Yoo, and E.-H. Song, “A new topology with high efficiency throughout all load range for photovoltaic PCS,” *IEEE Trans. Ind. Electron.*, vol. 56, no. 11, pp. 4427–4435, Nov. 2009.

[37] Y. Tang, P. C. Loh, P. Wang, F. H. Choo, F. Gao, and F. Blaabjerg, “Generalized design of high performance shunt active power filter with output LCL filter,” *IEEE Trans. Ind. Electron.*, vol. 59, no. 3, pp. 1443–1452, Mar. 2012.

[38] K.-J. Lee, J.-P. Lee, D. Shin, D.-W. Yoo, and H.-J. Kim, "A novel grid synchronization PLL method based on adaptive low-pass notch filter for grid-connected PCS," *IEEE Trans. Ind. Electron.*, vol. 61, no. 1, pp. 292–301, Jan. 2014.

[39] P. N. Enjeti and S. A. Choudhury, "A new control strategy to improve the performance of a PWM ac to dc converter under unbalanced operating conditions," *IEEE Trans. Power Electron.*, vol. 8, no. 4, pp. 493–500, Oct. 1993.

[40] Q. Song and W. Liu, "Control of a cascade statcom with star configuration under unbalanced conditions," *IEEE Trans. Power Electron.*, vol. 24, no. 1, pp. 45–58, Jan. 2009.

[41] P. Rioual, H. Pouliquen, and J. P. Louis, "Regulation of a PWM rectifier in the unbalanced network state using a generalized model," *IEEE Trans. Power Electron.*, vol. 11, no. 3, pp. 495–502, May 1996.

[42] S.-F. Chou, C.-T. Lee, P.-T. Cheng, and F. Blaabjerg, "A reactive current injection technique for renewable energy converters in low voltage ride-through operations," in *Proc. IEEE Power Energy Soc. Gen. Meet.*, Jul. 24–29, 2011, pp. 1–7.

[43] A. K. Thet and H. Saitoh, "Pitch control for improving the low-voltage ride-through of wind farm," in *Proc. Asia-Pacific Transmiss. Distrib. Conf. Expo.*, Oct. 26–30, 2009, pp. 1–4.

[44] A. Causebrook, D. J. Atkinson, and A. G. Jack, "Fault ride-through of large wind farms using series dynamic braking resistors (Mar. 2007)," *IEEE Trans. Power Syst.*, vol. 22, no. 3, pp. 966–975, Aug. 2007.

[45] E. R. Collins and R. L. Morgan, "A three-phase sag generator for testing industrial equipment," *IEEE Trans. Power Del.*, vol. 11, no. 1, pp. 526–532, Jan. 1996.

[46] Y. H. Chung, G. H. Kwon, T. B. Park, and G. Y. Lim, "Voltage sag and swell generator with thyristor controlled reactor," in *Proc. Int. Conf. Power Syst. Technol.*, 2002, vol. 3, pp. 1933–1937.

[47] M. Garca-Gracia, M. P. Comech, J. Salln, D. Lpez-Anda, and O. Alonso, "Voltage dip generator for wind energy systems up to 5 MW," *Appl. Energy*, vol. 86, no. 4, pp. 565–574, Apr. 2009.

[48] M. Yan and G. G. Karady, "A single-phase voltage sag generator for testing electrical equipments," in *Proc. IEEE Transmiss. Distrib. Conf. Expo.*, Apr. 21–24, 2008, pp. 1–5.

[49] A. O. Ibrahim, T. H. Nguyen, D.-C. Lee, and S.-C. Kim, "Ride-through strategy for DFIG wind turbine systems using dynamic voltage restorers," in *Proc. IEEE Energy Convers. Congr. Expo.*, Sep. 20–24, 2009, pp. 1611–1618.

[50] H. Shuju, L. JianLin, and X. Honghua, "Comparison of voltage sag generators for wind power system," in *Proc. Asia-Pacific Power Energy Eng. Conf*, Mar. 27–31, 2009, pp. 1–4.

[51] R. Lohde and F. W. Fuchs, "Laboratory type PWM grid emulator for generating disturbed voltages for testing grid connected devices," in *Proc. 13th Eur. Conf. Power Electron. Appl.*, Sep. 8–10, 2009, pp. 1–9.

[52] S. A. Richter, J. von Bloh, C. P. Dick, D. Hirschmann, and R. W. D. Doncker, "Control of a medium-voltage test generator," in *Proc. IEEE Power Electron. Spec. Conf.*, Jun. 15–19, 2008, pp. 3787–3793.

[53] C. Saniter and J. Janning, "Test bench for grid code simulations for multi-MW wind turbines, design and control," *IEEE Trans. Power Electron.*, vol. 23, no. 4, pp. 1707–1715, Jul. 2008.

Authors' photographs and biographies not available at the time of publication.